Available online at www.sciencedirect.com
ScienceDirect
Trans. Nonferrous Met. Soc. China 34(2024) 1081−1090
Transactions of Nonferrous Metals Society of China
www.tnmsc.cn

Preparation of interfacial metallurgically-bonded aluminum foam sandwich panels by graphite coating heat transfer technology

Xi SUN[1], Zhi-he DOU[1], Xi-xi SU[2], Peng HUANG[2], Qiang GAO[2], Zhan-hao FENG[2], Guo-yin ZU[2]

1. School of Metallurgy, Northeastern University, Shenyang 110819, China;
2. School of Materials Science and Engineering, Northeastern University, Shenyang 110819, China

Received 6 October 2022; accepted 19 July 2023

Abstract: An innovative approach that utilizes a graphite coating treatment (GCT) on precursors of aluminum foam sandwich (AFS) panels was proposed to improve heat transfer efficiency during the powder metallurgical foaming process. The heating and expansion characteristics, effects on cell structures and bending performance of different heat transfer methods were studied. The results indicated that the heating rates of precursors increased by approximately two-fold after applying GCT, resulting in improvements in the expansion ratio, cell size uniformity, and panel surface morphology of the AFS. Furthermore, the later stage of foaming featured a more consistent heating rate, increasing cell roundness and reducing microporous defects within cell walls. These advancements consequently bolstered the bending strength and energy absorption properties of AFS. Notably, GCT technology holds great potential for the production of large-format AFS, as the heat transfer rate remains unaffected by panel size.

Key words: aluminum foam sandwich; powder metallurgy foaming; efficient heat transfer; graphite coating treatment; cell structure

1 Introduction

Aluminum foam sandwich (AFS) panel is a novel composite material consisting of two outer metal sheets and a porous foam core [1]. In addition to possessing the light weight, energy absorption, and sound insulation properties of conventional porous materials, AFS exhibits excellent specific strength and stiffness [2−6]. When the interface achieves metallurgical bonding, the strength and serviceability of the AFS are further enhanced, making it an ideal material for integrating structure and functionality in many fields, including aerospace, transportation, and urban construction [7−9]. Multiple methods have been proposed for fabricating AFS with metallurgical bonding interfaces, such as hot-pressing [10,11], friction stir welding [12,13], and two-step foaming process [14]. Among them, powder metallurgy (PM) pack rolling technology is highly regarded to be particularly suitable for the preparation of large panels for engineering applications. However, the cell structure of aluminum foam prepared by PM is insufficient [15,16].

The inferior performance of cell structures primarily stems from the mismatch between the decomposition of the foaming agent and the melting of the matrix. During the early stages of foaming, when the liquid-to-solid phase ratio of the precursor is low, TiH_2 with a low decomposition temperature accumulates excessive hydrogen gas within the precursor, resulting in the formation of cell defects in the matrix. Various methods have been proposed to optimize the cell structure. HELWIG et al [17] and SUN et al [18] emphasized the importance of proper densification conditions for the precursor to enhance the cell structure. It was demonstrated that

Corresponding author: Guo-yin ZU, Tel/Fax: +86-24-83687372, E-mail: zugy@smm.neu.edu.cn
DOI: 10.1016/S1003-6326(23)66455-6

pre-oxidation treatment of the foaming agent can elevate the decomposition temperature, resulting in improved cell structure [19−22]. It was discovered that utilizing multiple alloy compositions as foaming substrates effectively lowered the melting point of the core powder, thereby mitigating pore defects [23−28]. Additionally, research indicated that increasing the heat transfer rate was crucial for improving cell structure [29].

However, enhancing the heat transfer efficiency during the engineering preparation process remains a formidable technical challenge. The conventional approach to increasing the heat transfer rate involves substantially raising the preset furnace temperature to boost the thermal radiation energy density [29−31]. However, this method has limitations, as the substantial temperature gradient between the foaming environment and the precursor in the later stages of foaming makes it challenging to control cell structure parameters. Moreover, it increases the risk of overheating the outer aluminum alloy plate of the AFS. LIN et al [32] addressed this by employing preheated molds to improve heat transfer efficiency through conduction to the precursor. Although this approach reduced the required furnace temperature, the preheating process of the molds decreased the preparation efficiency, making it unsuitable for industrial-scale production. Additionally, the choices of mold material, shape, and specifications directly affected the heating patterns of the precursor, adding complexity to the exploration of heating characteristics and limiting the applicability of the obtained experimental data for guiding the engineering preparation of AFS.

Therefore, it is necessary to develop a simplified and efficient heat transfer technology for preparing AFS at low foaming temperatures. In this study, we employed high thermal conductivity and heat-absorbing graphite to darken the precursor surface and investigated its impact on the heat transfer rate, cell structure of the core layer, and bending performance. Additionally, the heat transfer mechanism of the graphite coating treatment (GCT) technique and the advantages of this technique in the preparation of large-size AFS were elucidated.

2 Experimental

Figure 1 exhibits a schematic diagram of the AFS preparation process. The precursor was fabricated through PM using a rolling bonding technique. The raw material of the core was $AlSi_6Cu_4Mg_4$, which was composed of pure powder particles [33]. TiH_2 powders of the foaming agent were pre-oxidized in air at 470 °C for 3 h to delay decomposition. The 3003 aluminum alloy panels were welded with ER5356 flux to form the cavity shell. After filling it with mixed powders, two square tubes were riveted at both sides to seal the powders inside. Multistage rolling technology was employed to compact the core powder of the rolled precursor. The preferred rolling schedule with a lower reduction per pass was performed at room temperature to achieve homogeneous powder distribution and air removal. Subsequently, the

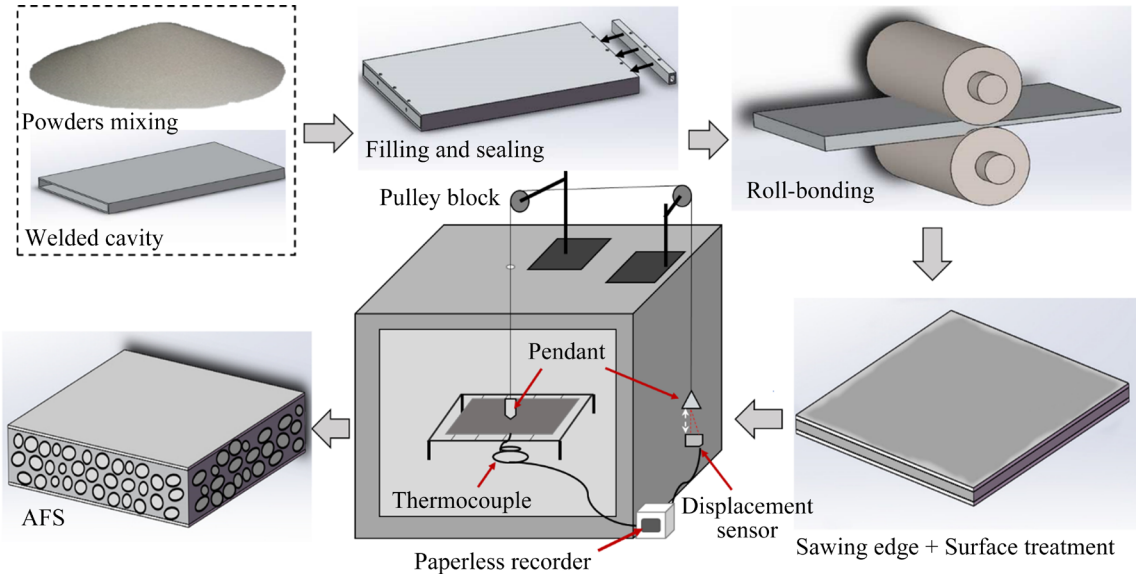

Fig. 1 Schematic diagram of AFS preparation process

precursor underwent the rolling process at a high deformation rate per pass in the temperature range from 300 to 400 °C, significantly improving the density of the core powder and achieving a close bond with the external panel. After edges were cut using an electric discharge machining (EDM), foam precursors with dimensions of 120 mm × 120 mm × 6.5 mm were prepared.

Before foaming, pre-treatment methods of no treatment and single/dual-sided blackening of the outer panel of precursors were adopted. The blackening substance was a viscous mixture of graphite powder (d_{90}≈2.6 μm) and heat-resistant coatings. The coating was ZS1011, which exhibited excellent wettability with graphite powder and aluminum alloy panels. After evenly coating the precursor surface with a brush, it was dried in air at room temperature.

A foaming device was designed in this laboratory and utilized to simultaneously measure the heating time, real-time temperature, and real-time expansion ratio of precursors throughout the foaming process. The temperature-measuring device was a thermocouple with a diameter of 1 mm. By shaping the armored thermocouple into a spring-like form, the temperature measurement point was in close contact with the lower panel of the precursor due to its elasticity, enabling accurate real-time temperature measurement. The height measuring device consisted of pulley blocks, asbestos wire, pendants, and a high-precision infrared displacement sensor, which achieved a low measurement error of repetition accuracy within ±35 μm. A hollow bracket was used as the foaming platform for precursors to minimize interference from the heat transfer medium.

Different foaming temperatures were adopted to heat precursors in this device. All the precursors were removed and cooled in air when their surface temperature reached 610 °C. Multiple replicate experiments were conducted for each foaming condition to ensure the validity of the data. Notably, the temperature field in the chamber wildly fluctuated when the furnace door was opened to place samples. Therefore, a temperature of 450 °C was chosen as the initial temperature measurement point, which was slightly lower than the pre-oxidation temperature of TiH_2. The AFS samples were cut using an EDM to obtain cross sections. After the surface was sprayed with black paint and then polished, the cell macrostructure was photographed with a digital camera and binarized using Image-Pro Plus software. The microscopic observations of the cell walls and composite interface were performed using an SSX−550 scanning electron microscopy (SEM). Repetitive three-point bending tests were conducted on AFS samples with a length of 120 mm and a width of 30 mm. The tests were performed using a span of 100 mm and a maximum compression displacement of 40 mm.

3 Results and discussion

3.1 Heating and expansion rate curves and cell structure

The heating and expansion rate curves of foam precursors with different faceplate treatments are depicted in Fig. 2. The green curve represents the untreated sample, while the red and black curves represent the samples with single-side GCT (S-GCT) and GCT, respectively. All precursors were foamed at 620 °C.

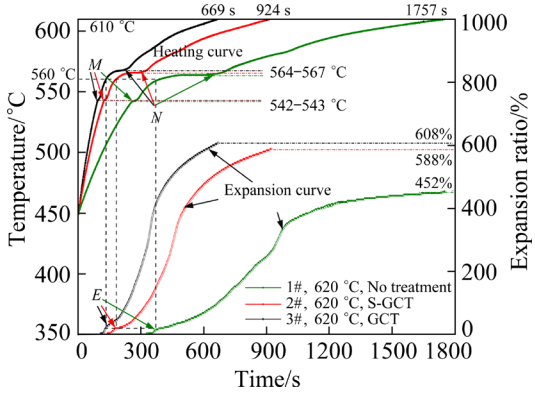

Fig. 2 Heating and expansion rate curves for AFS panels with different treatments

Similar patterns in heating and expansion behavior were obtained for these samples. The heating rate was larger in the early stages of foaming due to the considerable difference from the furnace temperature. Within the temperature range from 542 to 543 °C, a noticeable fluctuation was observed in the heating curve at the *M*-point. Partial core powder melting and absorption of heat energy decreased the heating rate at this moment. As the temperature approached approximately 560 °C, the precursors exhibited apparent expansion behavior, denoted as the *E*-point on the expansion curves. The

gas pressure that accumulated from the early decomposition of TiH_2 was reduced at this moment. Subsequently, the heating rate continued to decrease and approached zero at the *N*-point, within the temperature range from 564 to 567 °C. During this phase, all the heat radiation energy absorbed by the precursors transformed into energy required for the alloying process of the core powders. Afterward, the heating rate accelerated, and the matrix expansion rate significantly increased with temperature.

Three samples displayed notable differences in heating rates. More time was required for the untreated sample before the temperature reached the initial expansion *E*-point. The foaming duration of the untreated foam precursor was 1757 s when its temperature increased to 610 °C. As a comparison, the durations of foaming of the S-GCT and GCT samples were 924 and 669 s, respectively. The foaming duration decreased after their out-panels were blackened with graphite coating. The heating rate of the precursor increased approximately twofold after GCT in the same heating environment. Additionally, the expansion ratio of the precursors noticeably increased after GCT. The samples with GCT/S-GCT achieved high expansion ratios of 608% and 588%, respectively, while the expansion ratio of the untreated sample reached only 452%.

Figure 3(a) displays the cross section of AFS foamed using the aforementioned methods. Sample $1^{\#}$ displayed an uneven and inhomogeneous cell structure that was prepared from the untreated precursor. In contrast, the cell structures of Sample $2^{\#}$ and $3^{\#}$, foamed by S-GCT and GCT, were improved significantly with increasing heating rates. In addition, the solid layer on the boundary of Sample $1^{\#}$ was significantly thicker than that of the other samples. More internal gas overflowed from its edge with foaming duration extension, decreasing the expansion.

Figure 3(b) displays the panel morphologies of the above samples. A macroscopic darkening phenomenon, characteristic of overburning, was visible near the margin of Sample $1^{\#}$. A partial foam core layer with a large liquefaction ratio flowed out of the boundary and was combined with the lower panel. The darkened edges gradually disappeared when the duration of foaming decreased at the high-temperature stage, as observed in Samples $2^{\#}$ and $3^{\#}$.

GCT technology created a stable foaming environment for optimizing the cell structure. Figure 4 presents the heating and expansion rate curves of AFS fabricated under various foaming conditions, along with their corresponding cell structures. The Sample $5^{\#}$ was foamed at 680 °C with its surface unprocessed. For comparison, Sample $3^{\#}$ and $4^{\#}$ were foamed using GCT at 620 and 630 °C, respectively. Therefore, a similar foaming duration was obtained with the untreated precursor of Sample $5^{\#}$ by increasing the preset furnace temperature.

However, Sample $5^{\#}$ exhibited an insufficient heating rate in the early stages of foaming. The calculations revealed that the heating rate of Sample $5^{\#}$ below 50 °C before expansion was approximately 23 °C/min, significantly less than that of Sample $3^{\#}$ at 42 °C/min and Sample $4^{\#}$ at 45 °C/min. Furthermore, the temperature at the particular point (569 °C) on the curve of Sample $5^{\#}$ was much higher than that of Sample $3^{\#}$ (543 °C) and Sample $4^{\#}$ (549 °C), which should theoretically be identical for samples with the same powder composition. A more significant temperature

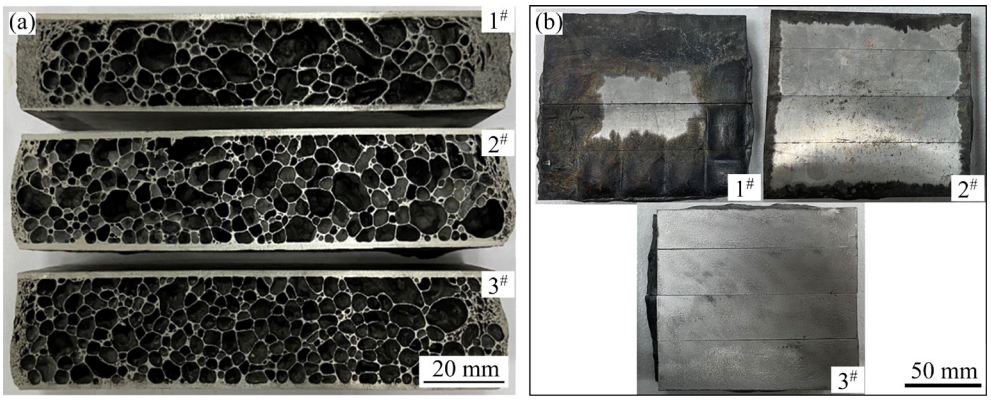

Fig. 3 Macrostructure of prepared AFS: (a) Cross section; (b) Panel morphology

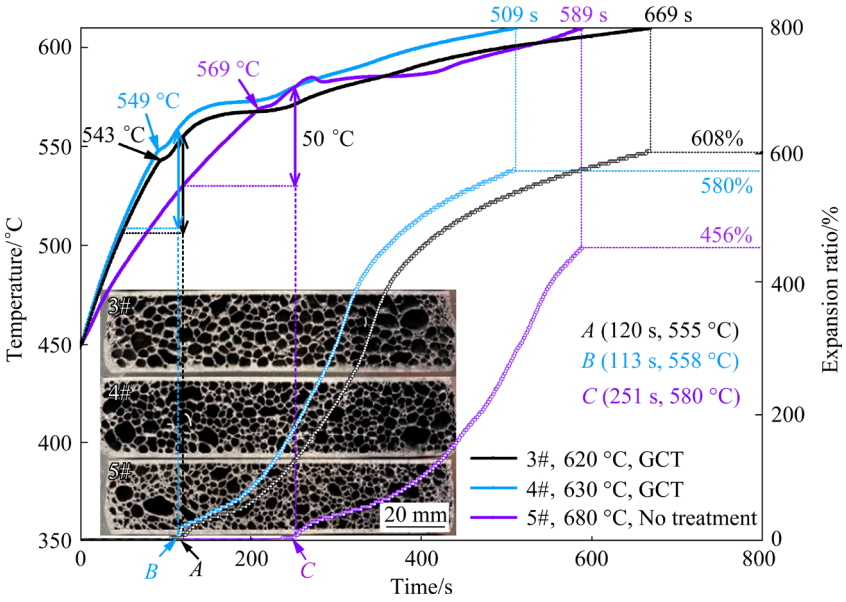

Fig. 4 Heating and expansion rate curves and cell structure of AFS foamed under various conditions

gradient was present between the measured outer panel and the foam core layer for the precursor at higher foaming temperatures. As a result, when the measured temperature reached 610 °C, the actual foam core temperature of Sample 5# was much lower than that of the others, resulting in the smallest expansion ratio.

Figure 5 provides the cell distribution statistics mentioned above. The average cell diameter of Sample 5#, measuring 3.55 mm, was significantly smaller than that of Samples 3# and 4#. The cell diameter decreased as the growth and merging stage duration diminished in the late stages of foaming. Homogeneity was assessed using the relative standard deviation (RSD), as the average cell diameter exhibited considerable variation. Sample 5# exhibited the worst cell homogeneity, with the highest RSD of 69%. The RSD decreased with increasing heating rate in the early stages of foaming. Additionally, the cell morphology of Sample 5# was irregular, with the smallest circular shape factor of 0.79. The circular shape of the cells was improved with increasing heating rate under the same cooling conditions.

The representative cell structure and composite interface morphology of the mentioned AFS are presented in Fig. 6. Figure 6(a) illustrates the typical cell structure features of Sample 1#, which underwent excessive foaming time in the late stage. The cell walls were the thinnest due to prolonged liquid-draining at high foaming temperatures. These

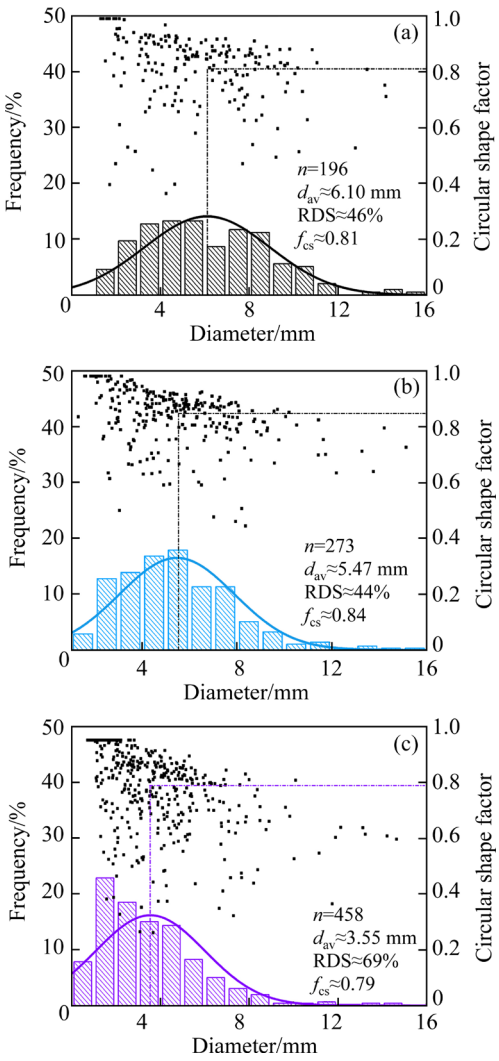

Fig. 5 Cell distributions of AFS samples: (a) 3#; (b) 4#; (c) 5#

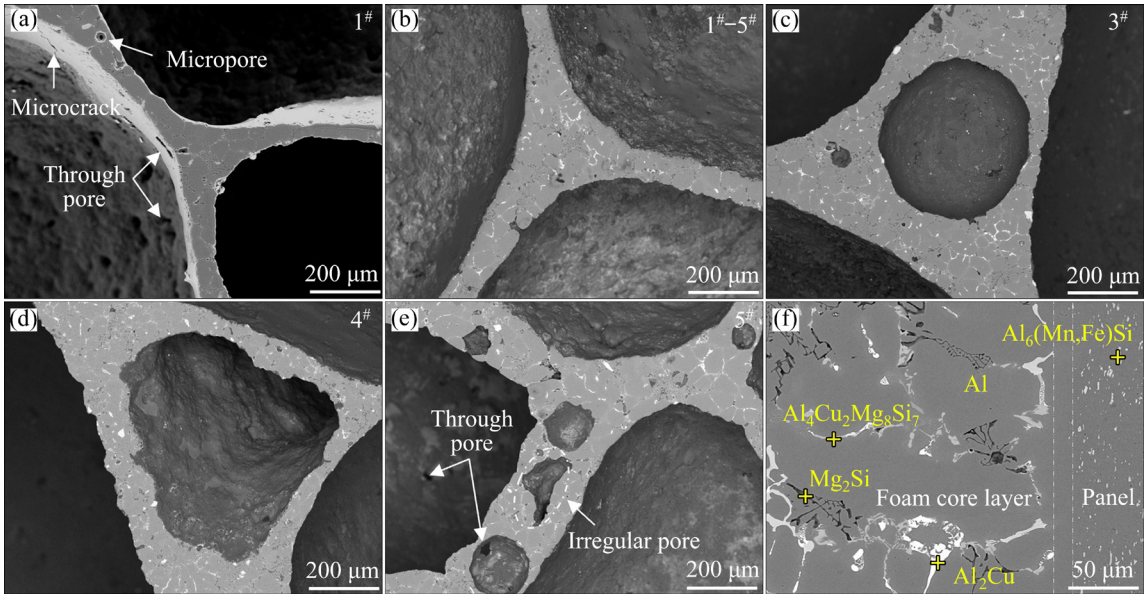

Fig. 6 Representative cell wall structures of samples (a−e) and microstructural characteristics of metallurgical bonding region (f)

thin cell walls lacked sufficient support and were prone to deformation during the cooling and shrinking process during the preparation of AFS, increasing the likelihood of microcracks and through-hole defects. Figure 6(b) shows the typical plateau boundary morphology that occurred locally in all the aforementioned AFSs. They exhibited a smooth cell wall and contained fewer micropores. Compared to Fig. 6(a), the support of the cell wall increased with increasing thickness. Figures 6(c, d) present the typical cell wall structures with visible micropores in the plateau boundaries of Sample 3# and 4#, respectively. The roundness of micropore in Sample 3#, which was foamed at a lower furnace temperature, was better than that of Sample 4#. Cell morphology was improved with extended foaming duration in the late foaming stage of high temperatures. Figure 6(e) shows the unique cell structure of Sample 5#, which had the briefest periods at high foaming temperatures. The shorter duration of liquid drainage resulted in thicker cell walls containing more micropores. Some micropore structures exhibited irregularities, and some were connected to the surrounding cells. Figure 6(f) provides a microscopic image of the junction between the panel and the foam core layer of the aforementioned AFS. The foam core consisted of Al-based, Mg_2Si, Al_2Cu, and $Al_4Cu_2Mg_8Si_7$ phases, while the panel consisted of Al-based and $Al_6(Mn,Fe)Si$ phases. The metallurgical bonding zone is the flat transition zone between the panel and the foam core layer, which consisted entirely of pure Al.

3.2 Bending and energy absorption properties

The results of the three-point bending test conducted on the mentioned AFS specimens are presented in Fig. 7. The peak load increased from 1.67 to 2.29 kN, and the energy absorption rose from 34.7 to 68.8 J for Samples 1# to 3#, which underwent different panel treatments under similar foaming conditions. Notably, after applying GCT, the AFS exhibited notable enhancements in flexural strength (with 37.1% improvement) and energy absorption properties (with 98.2% improvement). These parameters demonstrated further the improvement with an increasing heating rate, as in the case of Sample 4# (peak load: 3.07 kN, and energy absorption: 98.2 J). However, Sample 5#, which had an unprocessed panel surface and was exposed to the highest foaming temperature, underwent foam core fracturing at a compression displacement of 21.8 mm due to poor cell structure, resulting in a dramatic loss in flexural strength. Although Sample 5# achieved the highest peak load of 3.11 kN, the energy absorption performance was significantly weakened.

3.3 Heat transfer mechanism and advantages

GCT technology has significant advantages

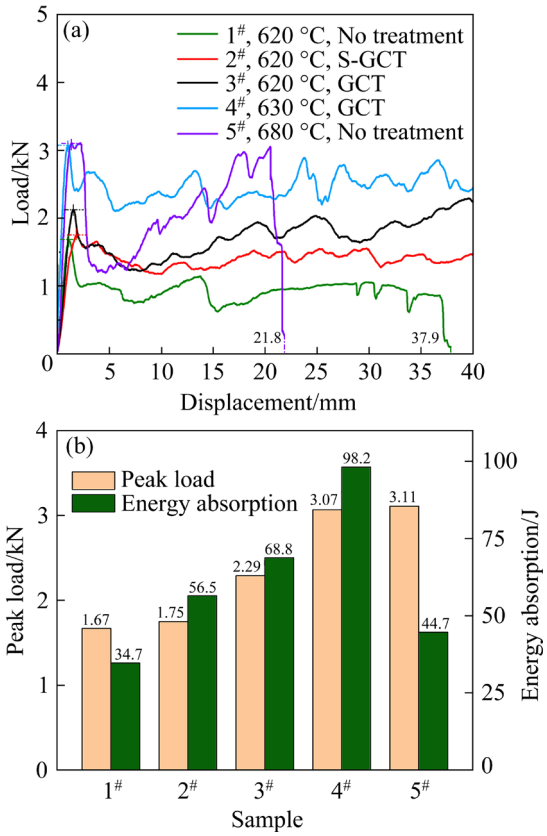

Fig. 7 Representative three-point bending test results for various AFSs: (a) Load–displacement curves; (b) Peak load and energy absorption

in the preparation of large-format AFS panels. Figure 8 illustrates the cell distributions of the AFS samples with three different specifications prepared using various heat transfer modes. Panel sizes of 60 mm × 60 mm, 120 mm × 120 mm, and 200 mm × 200 mm were arranged. The foam precursors underwent a heating process, employing three heat transfer methods arranged from top to bottom: untreated, utilizing a mold (a graphite plate of dimensions: 300 mm × 200 mm × 4 mm), and utilizing GCT technique. All samples were foamed in air at 620 °C for 16 min.

The cell structures of the three heat transfer methods exhibited distinct variations with increasing panel size. The AFS samples after GCT demonstrated an increased expansion ratio, while those samples without any auxiliary heat transfer method showed a decreasing trend. In the case of AFS samples with heat transfer enhanced by a mold, the expansion ratio initially increased and then decreased.

During the powder metallurgy foaming process, a portion of gas inevitably escapes from the surrounding boundary of an AFS panel. The proportion of the total area occupied by the edge decreases as its face-panel size increases. Consequently, a larger proportion of gas is retained within the foaming matrix for larger face-plates at the same heating rate, theoretically resulting in a higher expansion ratio of the AFS.

The variation pattern of AFS samples prepared by GCT aligned with the theoretical prediction. For faster heating rate conditions, the sample with dimensions of 200 mm × 200 mm exhibited a significantly larger expansion ratio of nearly 900% along with a uniform cell structure. Figure 9 illustrates the heat radiation energy distribution for different heat transfer methods. The blackened double-layer panels absorbed infrared radiation from the furnace and provided the majority of energy for the precursor, with the heating rate less affected by the panel size. The ultimate foaming temperatures were similar for AFS samples with different dimensions during the same foaming duration, resulting in similar cell diameters.

In comparison, due to the lower heat absorption efficiency of the untreated AFS outer plates, the effect of heat absorption at their periphery on the heating rate during the expansion process cannot be negligible. The heating rate slowed down as the proportion of the total area occupied by the periphery

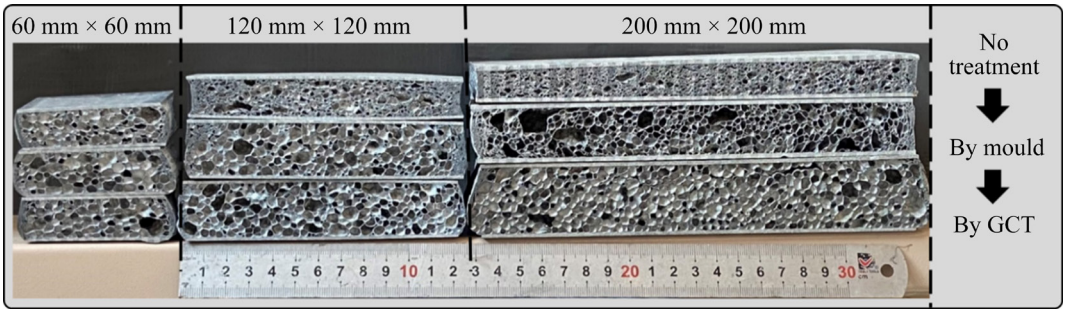

Fig. 8 Cell distributions of AFS samples with various sizes prepared by different heat transfer modes

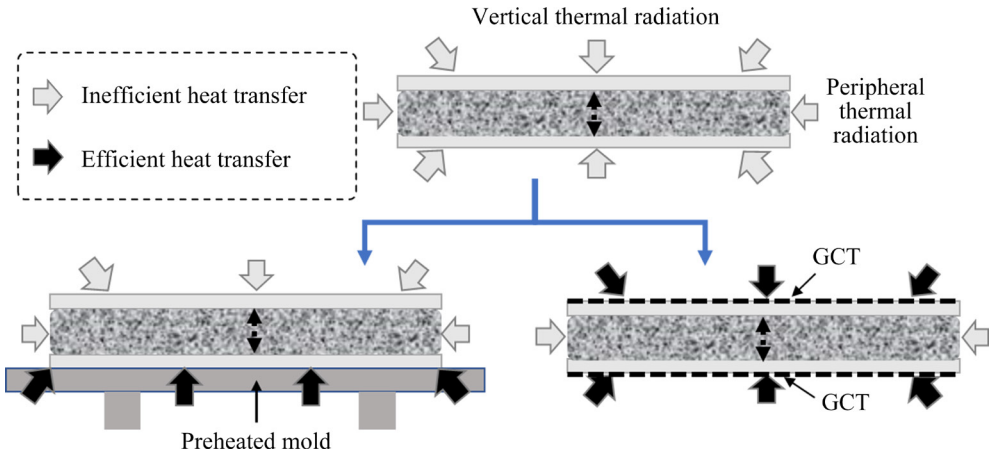

Fig. 9 Schematic diagram of distribution of heat radiation energy for different heat transfer methods

decreased with increasing panel size. As a result, the ultimate foaming temperature decreased, and the foaming duration of the later stage was shortened, leading to a decrease in the expansion ratio and average cell diameter. In the case of AFS samples treated with the same preheated mold, the heat transfer effect decreased with increasing the size of the foaming precursor. No adequate amount of heat transfer was provided to ensure a sufficient heating rate for the precursor with dimensions of 200 mm × 200 mm, resulting in a smaller expansion ratio and nonuniform cell structure of the AFS specimen.

4 Conclusions

(1) A rapid heating technology utilizing a graphite coating treatment (GCT) on precursors was proposed. This treatment resulted in an approximately twofold increase in the heating rate of the precursors, effectively reducing the suitable furnace temperature for foaming of AFS. The expansion ratio of the foam core, uniformity of cell sizes, and surface morphology of the panels were improved by using this technology.

(2) Compared with the conventional approach of raising the furnace temperature (680 °C) to improve the heat transfer rate, the GCT sample achieved a low preset furnace temperature of 620 °C while doubling the heating rate of the precursor before expansion and exhibiting a more stable heating rate during the later stages of foaming. Under the action of liquid drainage, the homogeneity of cell distribution was improved, along with the width and roundness of cells, while the micropores within cell walls were minimized.

(3) In the three-point bending test, the AFS prepared using the GCT precursor exhibited significant improvements in bending performance compared to the unprocessed panel AFS. The AFS prepared using GCT precursor achieved a peak load of 2.29 kN and energy absorption of 68.8 J, representing substantial increases of 37.1% and 98.2%, respectively, compared to the unprocessed panel AFS.

(4) GCT technology has great potential for applications in the production of large-sized AFSs due to its independent heat transfer rate, unaffected by sample size. This implies that AFSs of different sizes can achieve similar cell structures when exposed to the same furnace temperature.

CRediT authorship contribution statement

Xi SUN: Conceptualization, Methodology, Investigation, Visualization, Data curation, Formal analysis, Writing − Original draft, Writing − Review & editing; **Zhi-he DOU:** Conceptualization, Formal analysis, Writing – Review & editing; **Xi-xi SU:** Data curation, Formal analysis, Writing − Review & editing; **Peng HUANG:** Data curation, Writing − Review & editing; **Qiang GAO:** Writing − Review & editing; **Zhan-hao FENG:** Writing − Review & editing; **Guo-yin ZU:** Conceptualization, Project administration, Funding acquisition, Supervision, Writing − Review & editing.

Declaration of competing interest

The authors declare that they have no known competing financial interests or personal relationships that could have appeared to influence the work reported in this paper.

Acknowledgments

This work was supported by the National Natural Science Foundation of China (Nos. 52071069, U1332110), and the Liaoning Revitalization Talents Program, China (No. XLYC1902097)

References

[1] BANHART J, SEELIGER H W. Aluminium foam sandwich panels: Manufacture, metallurgy and applications [J]. Advanced Engineering Materials, 2008, 10(9): 793−802.

[2] XIA Xing-chuan, ZHANG Zan, ZHAO Wei-min, LI Chong, DING Jian, LIU Chen-xi, LIU Yong-chang. Acoustic properties of closed-cell aluminum foams with different macrostructures [J]. Journal of Materials Science & Technology, 2017, 33(11): 1227−1234.

[3] YU Hai-jun, YAO Guang-chun, WANG Xiao-lin, LIU Yi-han, LI Hong-bin. Sound insulation property of Al−Si closed-cell aluminum foam sandwich panels [J]. Applied Acoustics, 2007, 68(11/12): 1502−1510.

[4] HOU Wei-hong, ZHU Feng, LU Guo-xing, FANG Dai-ning. Ballistic impact experiments of metallic sandwich panels with aluminium foam core [J]. International Journal of Impact Engineering, 2010, 37(10): 1045−1055.

[5] LI Zhi-bin, LI Xue-yan, ZHENG Yu-xuan. Biaxial mechanical behavior of closed-cell aluminum foam under combined shear−compression loading [J]. Transactions of Nonferrous Metals Society of China, 2020, 30: 41−50.

[6] SALEHI M, MIRBAGHERI S M H, RAMIANI A J. Efficient energy absorption of functionally-graded metallic foam-filled tubes under impact loading [J]. Transactions of Nonferrous Metals Society of China, 2021, 31: 92−110.

[7] HUANG Peng, SUN Xi, SU Xi-xi, GAO Qiang, FENG Zhan-hao, ZU Guo-yin. Three-point bending behavior of aluminum foam sandwich with different interface bonding methods [J]. Materials, 2022, 15(19): 6931.

[8] PANTELAKIS S, TSERPES K I. Adhesive bonding of composite aircraft structures: Challenges and recent developments [J]. Science China−Physics Mechanics & Astronomy, 2014, 57(1): 2−11.

[9] SCHWINGEL D, SEELIGER H W, VECCHIONACCI C, ALWES D, DITTRICH J. Aluminium foam sandwich structures for space applications [J]. Acta Astronautica, 2007, 61: 326−330.

[10] LIN Hao, LUO Hong-jie, HUANG Wen-zhan, ZHANG Xiao, YAO Guang-chun. Diffusion bonding in fabrication of aluminum foam sandwich panels [J]. Journal of Materials Processing Technology, 2016, 230: 35−41.

[11] DING Xiang, LIU Yuan, WAN Tan. A novel hot-pressing method to prepare foamable precursor of aluminum foam sandwich (AFS) [J]. Materials Letters, 2020, 259: 126895.

[12] HANGAI Y, KAMADA H, UTSUNOMIYA T, KITAHARA S, KUWAZURU O, YOSHIKAWA N. Aluminum alloy foam core sandwich panels fabricated from die casting aluminum alloy by friction stir welding route [J]. Journal of Materials Processing Technology, 2014, 214(9): 1928−1934.

[13] WAN Long, HUANG Yong-xian, HUANG Ti-fang, LÜ Shi-xiong, FENG Ji-cai. Novel method of fluxless soldering with self-abrasion for fabricating aluminum foam sandwich [J]. Journal of Alloys and Compounds, 2015, 640: 1−7.

[14] LU Xiao-tong, LUO Hong-jie, YANG Shi-jie, WEI You, XU Jian-rong, YAO Zhi. Two-step foaming process combined with hot-rolling in fabrication of an aluminium foam sandwich panel [J]. Materials Letters, 2020, 265: 127427.

[15] RACK A, HELWIG H M, BüTOW A, RUEDA A, MATIJAŠEVIĆ-LUX B, HELFEN L, GOEBBELS J, BANHART J. Early pore formation in aluminium foams studied by synchrotron-based microtomography and 3-D image analysis [J]. Acta Materialia, 2009, 57: 4809−4821.

[16] HEIM K, VINOD-KUMAR G S, GARCíA-MORENO F, RACK A, BANHART J. Stabilisation of aluminium foams and films by the joint action of dispersed particles and oxide films [J]. Acta Materialia, 2015, 99: 313−324.

[17] HELWIG H M, HILLER S, GARCIA-MORENO F, BANHART J. Influence of compaction conditions on the foamability of AlSi8Mg4 alloy [J]. Metallurgical and Materials Transactions B−Process Metallurgy and Materials Processing Science, 2009, 40(5): 755−767.

[18] SUN Xi, HUANG Peng, ZHANG Xiao-guang, HAN Nan-ding, LEI Jin-qin, YAO Yong-tao, ZU Guo-yin. Densification mechanism for the precursor of AFS under different rolling temperatures [J]. Materials, 2019, 12(23): 3933.

[19] DING Xiang, LIU Yuan, CHEN Xiang, ZHANG Hua-wei, LI Yan-xiang. Optimization of cellular structure of aluminum foams produced by powder metallurgy method [J]. Materials Letters, 2018, 216: 38−41.

[20] LI Xun, LIU Ying, YE Jin-wen, AN Xu-guang, CAO Zhi-nan, LIU Xiao-bo. Innovative surface modification of TiH_2 to fabricate aluminum foam with enhanced mechanical properties [J]. Materials Letters, 2018, 210: 350−353.

[21] MATIJASEVIC-LUX B, BANHART J, FIECHTER S, GÖRKE O, WANDERKA N. Modification of titanium hydride for improved aluminium foam manufacture [J]. Acta Materialia, 2006, 54: 1887−1900.

[22] MATIJASEVIC B, BANHART J. Improvement of aluminium foam technology by tailoring of blowing agent [J]. Scripta Materialia, 2006, 54: 503−508.

[23] DING Xiang, PENG Bo, HU Xing-sheng, PAN Kai-kai, LIU Yuan, WAN Tan, RAN Song-lin. Effect of Cu and Sn additions on the cellular structure of Al−Si−Mg alloys foaming at low temperature (≤600 °C) [J]. Composites Part B: Engineering, 2022, 234: 109693.

[24] HELWIG H M, GARCIA-MORENO F, BANHART J. A study of Mg and Cu additions on the foaming behaviour of Al−Si alloys [J]. Journal of Materials Science, 2011, 46(15): 5227−5236.

[25] DENG Fan, FAN Jian-zhong, LIU Yan-qiang, LU Xue-han, WEI Shao-hua, NIE Jun-hui. Effect of Cu on pore structure of Al−Si foam [J]. Metals and Materials International, 2021, 27(12): 5239−5246.

[26] BHOGI S, MUKHERJEE M. Foam stabilization by magnesium [J]. Materials Letters, 2017, 200: 118−120.

[27] AGUIRRE-PERALES L Y, JUNG I H, DREW R A L. Foaming behavior of powder metallurgical Al−Sn foams [J]. Acta Materialia, 2012, 60: 759−769.

[28] VINOD-KUMAR G S, HEIM K, JERRY J, GARCIA-

MORENO F, KENNEDY A R, BANHART J. Effect of magnesium addition on the cell structure of foams produced from re-melted aluminum alloy scrap [J]. Metallurgical and Materials Transactions B−Process Metallurgy and Materials Processing Science, 2017, 48(5): 2551−2563.

[29] KIM A, TUNVIR K, NAHM S H, CHO S S. Time-temperature superposition for foaming kinetics of Al-alloy foams [J]. Journal of Materials Processing Technology, 2008, 202(1/2/3): 450−456.

[30] DENG Fan, LIU Yan-qiang, LU Xue-han, FAN Jian-zhong. Improved stability of aluminum foam through heat treatment of foamable precursor [J]. Metals and Materials International, 2020, 26(10): 1596−1601.

[31] ASAVAVISITHCHAI S, KENNEDY A R. The effect of Mg addition on the stability of Al−Al_2O_3 foams made by a powder metallurgy route [J]. Scripta Materialia, 2006, 54: 1331−1334.

[32] LIN Hao, LUO Hong-jie, ZHANG Zhi-gang, MA Jun-fei, YAO Guang-chun. Study on improvement of aluminum foams by rapid foaming [J]. Materials Letters, 2017, 188: 288−290.

[33] RAGHAVAN V. Al−Cu−Mg−Si (aluminum−copper−magnesium−silicon) [J]. Journal of Phase Equilibria and Diffusion, 2007, 28(2): 198−200.

基于石墨涂层传热技术制备界面冶金结合泡沫铝夹芯板

孙 溪[1]，豆志河[1]，苏喜喜[2]，黄 鹏[2]，高 强[2]，冯展豪[2]，祖国胤[2]

1. 东北大学 冶金学院，沈阳 110819；
2．东北大学 材料科学与工程学院，沈阳 110819

摘　要：提出一种通过石墨涂敷处理(GCT)泡沫铝夹芯板(AFS)前驱体来提高其在粉末冶金发泡过程中传热效率的新方法。研究不同传热方法的升温和膨胀特征以及对泡孔结构和抗弯性能的影响。结果表明，前驱体在采用 GCT 后，升温速度增加近 2 倍，这提高了 AFS 的膨胀率、改善了泡孔尺寸均匀性和外部面板形态。此外，在发泡后期阶段具有更加平稳的升温速率，这有助于提高泡孔圆度，并减少泡壁内微孔缺陷。这些改变使 AFS 的弯曲强度和吸能性能得以显著提高。值得注意的是，因为热传递速率不受板幅尺寸的影响，GCT 技术在大尺寸 AFS 的生产中具有巨大潜力。

关键词：泡沫铝夹芯板；粉末冶金发泡；高效传热；石墨涂敷处理；泡孔结构

(Edited by Bing YANG)